

A mobile tram system for systematic sampling of ecosystem optical properties

John A. Gamon*, Yufu Cheng, Helen Claudio, Loren MacKinney, Daniel A. Sims

*Department of Biological Sciences and Center for Environmental Analysis, California State University, Los Angeles,
5151 State University Drive, Los Angeles, CA 91030, USA*

Received 18 March 2006; received in revised form 1 April 2006; accepted 2 April 2006

Abstract

Reliable and repeatable field sampling methods are needed for monitoring ecosystem optical properties linked to carbon flux. Here we describe a tram system, consisting of a dual-detector spectrometer mounted on a robotic cart for mobile sampling of ecosystem spectral reflectance. To illustrate the application of this system for monitoring dynamic ecosystem activity, we illustrate how the tram can be used for exploring the multiple factors influencing the Normalized Difference Vegetation Index (NDVI), a measure of vegetation greenness and a key optical indicator of vegetation carbon dioxide assimilation. With this system, we collected five years of NDVI data for a chaparral ecosystem in Southern California subject to extreme disturbance. Key factors affecting NDVI at this site included snow cover, sky conditions (clear vs. cloudy), time of day, season, species composition, and environmental perturbations such as rainfall, drought and fire. Applications of this tram system include ecosystem monitoring, satellite validation, and developing surface-atmosphere flux models from remote sensing.

© 2006 Elsevier Inc. All rights reserved.

Keywords: Robotic tram system; Spectral reflectance; NDVI; Disturbance; Chaparral; FLUXNET; SpecNet

1. Introduction

The exchanges of carbon dioxide and water vapor between terrestrial ecosystems and the atmosphere exert large impacts on the global carbon and water cycles, and are critical to the regulation of the Earth's climate. We now have a large set of tools for measuring these fluxes, each with a particular set of strengths and limitations. Eddy covariance can measure whole ecosystems, but the sampling region is limited to a relatively small "footprint" (typically a few hectares or less) and cannot readily isolate the contribution of component parts (Moncreiff et al., 1996). Other methods, including inversion models utilizing the flask sampling network (Tans et al., 1990) and satellite remote sensing (Running et al., 2004), provide synoptic coverage for large regions of the globe, but cannot directly resolve local or regional fluxes, and are inherently difficult to compare to point sampling methods operating at much finer scales.

One reason for the lack of comparability lies in the different sampling domains—space and time. Flux towers provide a direct means of measuring surface-atmosphere fluxes of carbon dioxide and water vapor (Baldocchi et al., 1988). They sample a fluctuating region (footprint) through time from a discrete geographic point, so they cannot directly resolve spatial patterns. Additionally, they are costly, limited to relatively flat, uniform terrain, and cannot readily be installed at all sites, leaving much of the world unsampled (Running et al., 1999). This undersampling problem is often tackled by remote sensing, which can provide synoptic coverage of large regions or the whole earth, but can be difficult to compare the point measurements provided by flux towers (Cheng et al., 2006-this issue).

Typically, remote measurements of spectral reflectance are used to calculate "vegetation indices" (e.g. the Normalized Difference Vegetation Index), which are then used in models to estimate carbon fluxes (e.g. Running et al., 2004). Remote sensing traditionally provides an image for a defined period or discrete point in time, but again with some loss of spatial resolution, depending upon the pixel size. Frequent global satellite coverage (e.g. the MODIS sensors on the Aqua and Terra

* Corresponding author.

E-mail address: jgamon@gmail.com (J.A. Gamon).

platforms) now provides repeat imagery, but at such large pixel sizes (250 to 1000 m²) that direct comparison with point sampling methods (e.g. eddy covariance) presents formidable challenges. Models and scaling methodologies can be used to try to “fill the gap,” but the large spatial scale of most satellite sampling makes this difficult.

To validate satellite data and link them to flux towers, ground-based methods at the appropriate temporal and spatial scales are needed. Portable spectrometers are widely available for field measurements, but most manual field methods cannot easily sample a region sufficiently representative of the flux tower footprint or satellite pixel. Besides, extensive manual sampling is often undesirable because the human presence can disturb the flux tower measurements. Aircraft platforms can help relate field and satellite methods (e.g. Cheng et al., 2006-this issue; Fuentes et al., 2006-this issue), but usually do not provide sufficient temporal coverage for comparison with continuous flux sampling, and consequently miss key transitions in ecosystem behavior associated with disturbance and stress.

The pressing need to understand ecosystem-atmosphere fluxes requires that we integrate this diverse array of methods and tools, particularly if we are to develop defensible calibrations for remote sampling methods and understand factors controlling surface-atmosphere fluxes. This integration of optical and flux measurements is a primary goal of SpecNet (Spectral Network), a cooperative network of investigators and field sites where scale-appropriate optical remote sensing is being developed and applied to understanding fluxes and other key ecosystem processes (Gamon et al., 2006-this issue). Yet, integration poses formidable technical challenges due to the multiple scales, methods, sampling domains, and data formats of flux and optical methods.

One way to meet this challenge is to develop “mid-range,” optical sampling platforms, intermediate in scale between the MODIS pixel and the hand-held field spectrometer. For this purpose, we have designed and deployed a novel “tram system” consisting of a robotic cart carrying optical and other environmental sensors that sample at a spatial and temporal scale similar to that of the flux tower footprint. By providing optical remote sensing data at this scale, this mobile tram system was specifically designed to facilitate integration of optical and flux data for the purpose of developing improved flux models, understanding the controls on ecosystem-atmosphere carbon and water vapor fluxes, and validating satellite data products, all of which are key SpecNet objectives (Gamon et al., 2006-this issue).

Most models of ecosystem-atmosphere carbon flux that utilize remote sensing depend upon the Normalized Difference Vegetation Index (NDVI), a widely used index of vegetation “greenness” that is commonly obtained from satellite or aircraft spectrometers. Typically, the NDVI (or similar measures of vegetation greenness) is derived from reflectance in red and near-infrared wavebands, and is used to estimate spatial and temporal patterns of CO₂ flux for terrestrial ecosystems (Gamon & Qiu, 1999; Running et al., 2004). But the NDVI can be affected by many factors, some of which can potentially confound models of carbon flux (Malmstrom et al., 1997;

Sellers et al., 1996). Here we describe the design and operation of the tram system, and present results illustrating how several factors can influence the Normalized Difference Vegetation Index (NDVI) in a highly dynamic chaparral ecosystem.

2. Methods

The tram system described here was installed at Sky Oaks in San Diego County, CA, USA (33° 22' 26.0" N, 116° 37' 22.4" W). This site includes a flux tower, operated by the Global Change Research Group at San Diego State University, and is part of the FLUXNET network (Baldocchi et al., 2001). The vegetation of this site is comprised primarily of montane chaparral, with *Adenostema fasciculatum* (chamise), *Adenostema sparsifolium* (redshank), *Arctostaphylos pungens* (manzanita) and *Ceanothus greggii* (ceanothus) as dominant shrub species (Stylinski et al., 2002). The climate is Mediterranean, characterized by cool, wet winters and hot, dry summers, with most of the rainfall falling between December and June. The region is subject to periodic drought and wildfire, leading to a highly dynamic ecosystem that undergoes occasionally profound shifts in species composition and ecosystem-atmosphere fluxes.

The tram rail design was inspired by a track system originally developed and deployed at Oak Ridge, Tennessee and the boreal forest for below-canopy radiation sampling (Baldocchi et al., 2000), but redesigned here for above-canopy sampling. At our site, the tram track consisted of 2-m sections of 0.48 cm × 3.8 cm (3/16 in. × 1.5 in.) angle aluminum, spaced 27.3 cm (10.75 in.) apart, joined with 0.635 cm (1/4 in.) thick metal connector plates and cross bars. The track is readily available from standard extruded aluminum components, and can be quickly disassembled into 2-m segments for shipping (e.g. in PVC drainage tubes). Depending on the particular stand structure, the track can be mounted on any of a number of supports. For quick deployments in short-statured vegetation, we use portable commercial tripods that range in height from 0 to 5 m above the ground (Fig. 1). This design allows ready assembly and disassembly, and accommodates topographic variation by extending the adjustable tripod legs and masts. For more permanent and lower cost installations, the tripods can be replaced by wooden posts supported by guy wires.

The standard track length is approximately 100 m, which is typically placed near the primary footprint of an eddy covariance tower. This length was determined in part by the requirement to sample a representative segment of a flux tower footprint (typically one to several hectares) and by the desire to conduct geo-statistical analyses of the scale-dependence of ecosystem optical properties (Rahman et al., 2003). Additionally, a standardized 100-m track length and regular sampling lag (typically 1-m intervals or less) facilitates both repeated measurement of the same ecosystem and direct comparison of contrasting ecosystems, meeting the sampling objectives of the SpecNet network (Gamon et al., 2006-this issue).

The core instrument on the cart is a dual-detector spectrometer (UniSpec DC, PP Systems, Amesbury MA, USA) that simultaneously samples downwelling and upwelling radiation (Fig. 1), allowing calculation of surface reflectance, and real-time

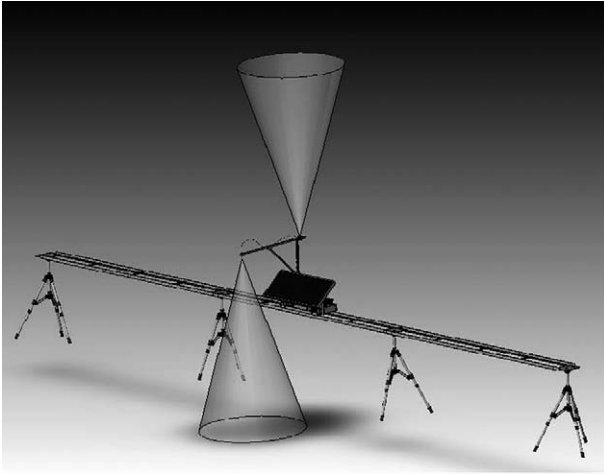


Fig. 1. Schematic of tram system, showing cart traversing the ecosystem on an elevated rail. Using upward- and downward-pointing foreoptics, a dual-detector spectrometer enables simultaneous sampling of upwelling and downwelling radiation (illustrated by cones), providing “on-the-fly” correction for changing sky conditions needed for accurate calculation of spectral reflectance. Note that the actual field-of-view typically differs from that shown here and is determined by the exact foreoptics (see text for further details).

correction for changing sky condition, including clouds. Each detector contains 256 bands ranging from approximately 310 nm to approximately 1130 nm, and the two detectors are approximately matched in their spectral range and bandwidth. While nominal bandwidth (band-to-band spacing) is approximately 3 nm, the actual bandwidth (full-width-half-maximum for each band) for these detectors is approximately 10 nm. The upward-looking detector is fitted with a fiber optic (UNI686, PP Systems, Amesbury MA, USA) and cosine head (UNI435, PP Systems, Amesbury MA, USA) mounted on the cart mast or boom and samples downwelling irradiance, thus providing a “reference” channel needed for reflectance calculation and for monitoring

changing sky conditions. In typical usage, the downward-looking channel is fitted with a fiber optic (UNI684, PP Systems, Amesbury MA, USA) and a field-of-view restrictor (“hypo-tube”—UNI688, PP Systems, Amesbury MA, USA) that effectively limits the field of view to approximately 20° (e.g. from a distance of 3 m, this samples a region on the ground of approximately 1 m). Optional foreoptics (not used in this study) include lenses with particular fields-of-view. Typically, the downward-looking foreoptic is mounted in a nadir (vertical) orientation, and this orientation can be easily modified for different purposes.

The cart dimensions are approximately 30 by 61 by 46 cm (12×24×18 in.), and accommodate the spectrometer, datalogger, computer, and power supply (a lead-acid battery, typically 3 Ah, 12 V). To maintain battery power, a solar panel and charger can be fitted on the top of the cart and tilted to optimize insolation (Figs. 1 and 2). Additionally the cart supports an adjustable mast and boom, typically configured with several sensors including the spectrometer’s downward and upward-pointing foreoptics, an infrared thermometer for surface temperature (IRTS-P, Apogee Instruments Inc., Logan UT, USA), air temperature sensors (type T thermocouples, Omega, Stamford CT, USA), relative humidity sensors (HTM2500, Digikey, Thief River Falls, MN, USA), quantum sensors (LI-190, LI-COR, Lincoln, NE, USA) and pyranometers (LI-200, LI-COR, Lincoln, NE, USA). Periodic addition of an optional digital camera (CoolPix 5400, Nikon, Tokyo, Japan) provides a photographic record of the landscape as it is being sampled by the cart sensors (see Fig. 7, below).

Together, the basic cart components provide a flexible and modular system that can be readily reconfigured for different sampling needs. The cart and sensors can be operated in several modes. In fully manual mode, the motor can be disconnected and the cart can be pushed along the track as a mobile platform for repeated, manual sampling. In semi-automatic mode, the system

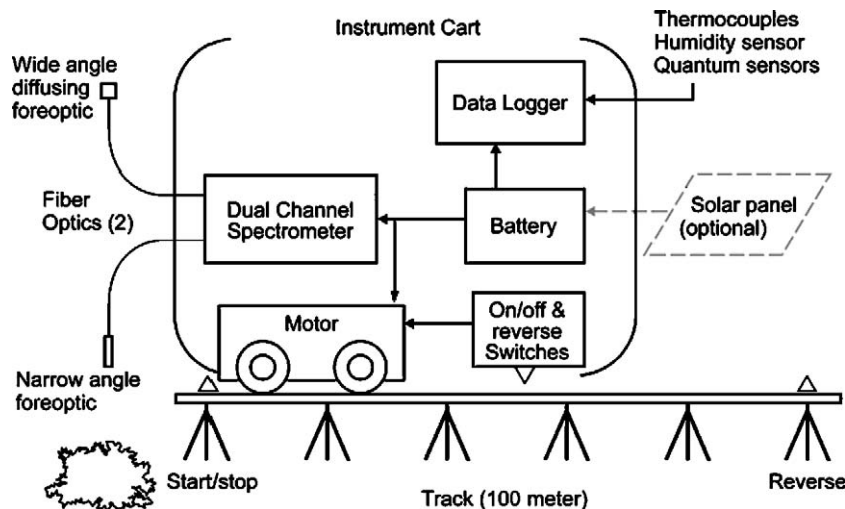


Fig. 2. Schematic of tram components, consisting of 100-m track with 1-m position markers (not shown) and end markers (triangles). The cart is driven by a motor directed by on/off and reverse switches triggered by end markers (pointed triangles). To determine surface reflectance under changing sky conditions, a dual-channel spectrometer simultaneously samples upwelling and downwelling radiation with a set of upward- and downward-looking foreoptics. Also shown are a datalogger and optional environmental sensors for sampling of additional ecosystem surface and micrometeorological properties (e.g. surface and air temperature, relative humidity, and incoming broadband radiation).

can be started by an operator, and the cart travels unattended down the track, reverses at the far end upon sensing a reversing marker, then returns to the original location, and shuts down automatically upon sensing an end-track marker. In fully automatic mode, the cart can be started and stopped remotely using a wireless link (Wireless Moxa serial-to-WiFi Ethernet transceiver Moxa Technologies, Inc., Brea, CA, USA) to the on-board computer that triggers the motor controller to start or stop cart motion and sampling. A key element for automatic mode is the motor controller (BS2-IC, Parallax, Rocklin, CA, USA) that can also be programmed to control the motor speed, and trigger the cart sampling based on input from track sensors or the computer time clock. In typical operation, the cart is operated at a speed of approximately 10 m per min, allowing the cart to traverse the full track length in 10 min.

Typically, cart sensors can be operated any of several ways. In fully manual mode, sensors can be triggered by the user via the keyboard of the onboard spectrometer or datalogger. However, this requires full user access to the cart, which is often impossible at many sites due to dense or tall vegetation, standing water, or other factors. Another common reason for avoiding manual sampling is the desire to avoid artifacts of human disturbance such as trampling vegetation or breathing when upwind of an eddy flux tower. In automatic or semi-automatic mode, the sensors can be programmed via the on-board computer, datalogger or motor controller to be triggered either on a pre-set time interval (time-sampling mode) or by pre-set metal distance markers (position-sampling mode), typically positioned at each meter along the track. In position-sampling mode, these markers deflect a switch (Omron D4C-1620, Digikey, Thief River Falls MN, USA) mounted on the bottom of the cart chassis as the cart passes each marker. In position-sampling mode (using the distance markers as position triggers), the instruments sample at identical locations through time, whereas in time-sampling mode, exact position replication is not possible, but can be approximated in software via interpolation of adjacent samples. In both sampling modes, the cart instruments are triggered either by the switch (position mode) or the on-board datalogger time clock (time mode).

Software includes separate components for datalogger control (23X Campbell Scientific, Logan UT, USA), spectrometer control and data processing (UniSpecDC, PP Systems, Amesbury Mass, USA) and tram motor control (BS2-IC, Parallax, Rocklin, CA, USA). On-board data processing is normally limited to uncalibrated radiance and irradiance calculation using input from the two spectrometer detectors. Final data processing typically occurs “offline” using software (Multispec, available from the authors, or from PP Systems, Amesbury MA, USA) that calculates exact waveband position for each detector separately, interpolates values to user-determined spectral intervals (typically each nanometer), then divides the upwelling (reflected) signal at each wavelength by the corresponding downwelling (irradiance) signal at each wavelength to obtain a “raw” reflectance (Fig. 4A, below). For final reflectance calculation, this ratio can be further corrected by a cross-calibration spectrum (Fig. 4B, below) obtained by comparing the irradiance (downwelling) signal to the radiance (upwelling) signal of a 99% reflective white standard panel

(Spectralon, Labsphere Inc., North Sutton, NH), yielding a corrected reflectance spectrum (Fig. 4C, below). This procedure is summarized in Eq. (1).

$$R_{\text{corrected}} = (I_{\text{target}}/I_{\text{downwelling}}) * (I_{\text{downwelling}}/I_{\text{panel}}) \quad (1)$$

Where $R_{\text{corrected}}$ refers to the corrected reflectance. The first term ($I_{\text{target}}/I_{\text{downwelling}}$) is the raw (uncorrected) reflectance spectrum calculated by dividing the response of the downward-looking detector (positioned over a target) by the response of the upward-looking sensor (measuring downwelling irradiance). The second term ($I_{\text{downwelling}}/I_{\text{panel}}$) is the cross-calibration spectrum calculated by dividing the response of the upward-looking sensor by the response of the downward-looking sensor when the instrument is positioned over the white calibration panel. This procedure is also illustrated graphically in Figs. 3, 4, below.

Ideally, cross-calibrations are obtained under similar sky and sun angle conditions as the actual measurements by placing the white panel at the end-track (start or stop) position. Since a full round-trip on the track typically takes approximately 20 min, under clear-sky conditions, reflectance can also be approximated by dividing the upwelling signal of a target surface (soil or vegetation) by the upwelling signal of the closest panel sample. However, in routine application, reflectance spectra are

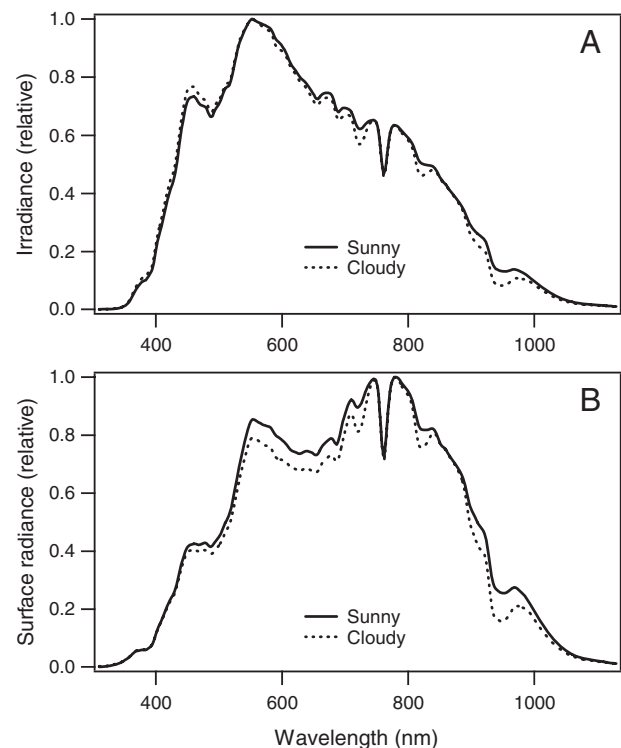


Fig. 3. Examples of raw data from the dual-detector spectrometer on the tram, consisting of downwelling solar irradiance (A) and upwelling surface radiance (B). Data were obtained on a sunny day (October 16, 2002) and a cloudy day (October 17, 2002) near 13:00 local time (approximately solar noon). Spectra are expressed in uncalibrated, relative units, normalized to a maximum value of one (for ease of visualization) and represent averages of over 200 spectra collected along a 100-m tram transect over approximately 20 min.

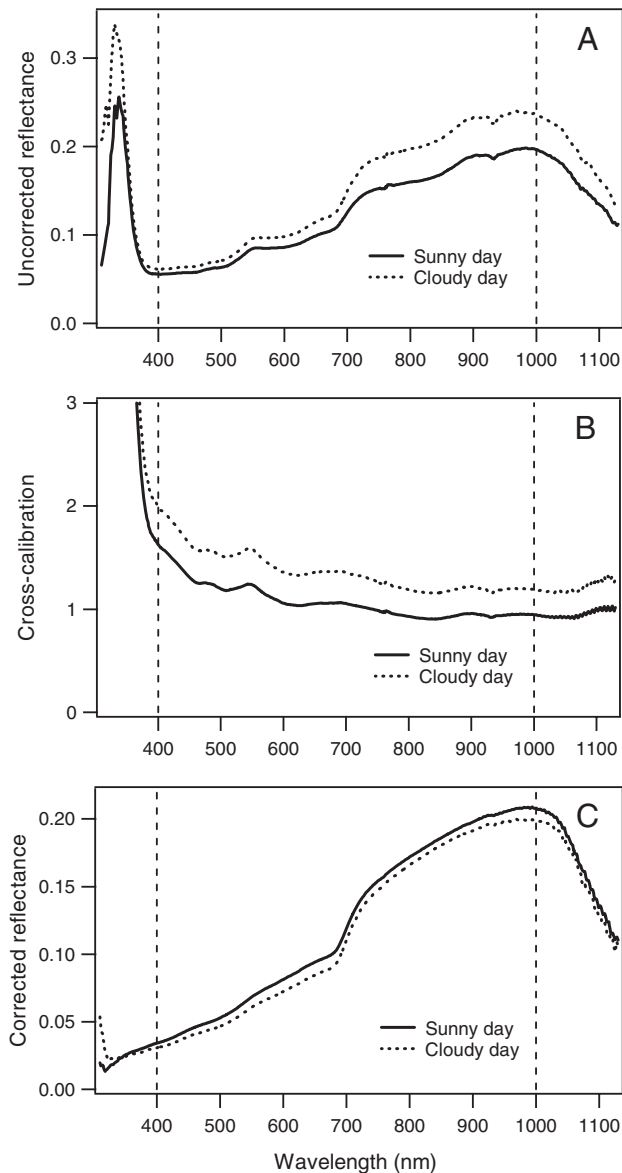


Fig. 4. Procedure for obtaining a corrected reflectance spectrum from the raw spectra (Fig. 3) collected from the dual-detector spectrometer. First, the upwelling uncalibrated target radiance (Fig. 3B) is divided by the downwelling uncalibrated sky irradiance (Fig. 3A), yielding uncorrected (raw) reflectance (A). This spectrum is then multiplied by the appropriate cross-calibration spectrum (B), which is expressed as a ratio of the upward- and downward-looking spectrometer channels when the instrument foreoptics are positioned over a white calibration target (see Eq. (1)). The resulting corrected reflectance spectrum (C) removes artifacts (minor peaks and dips) associated with sensor and foreoptics. In this case, the spectra represent average reflectance spectra for the entire 100 m transect. Vertical dashed lines (400 and 1000 nm) indicate the limits of acceptable data; values below and above these wavelengths are of questionable validity due to weak signal to noise.

calculated using the cross-calibration procedure described in Eq. (1) and illustrated in Figs. 3 and 4.

Reflectance spectra from the tram transect can be used to calculate vegetation indices in one of two ways. In one way, an index is calculated from the reflectance value for each 1-m tram sampling position (each “small pixel”), representing the variation along the sampling transect (e.g. Fig. 6, below). In the second way, an average transect reflectance is first calculated (simulating

a “big pixel”), and an index is then calculated from the average transect reflectance (e.g. Fig. 10, below).

In this study, the Normalized Difference Vegetation Index (NDVI) was calculated from corrected reflectance in red and near infrared wavelengths using the following formula:

$$\text{NDVI} = (R_{\text{NIR}} - R_{\text{RED}}) / (R_{\text{NIR}} + R_{\text{RED}}) \quad (2)$$

In this particular study, we used a narrow-band NDVI with 680 nm as the red waveband and 800 nm as the NIR waveband.

3. Results

Sky conditions (clear vs. overcast) had a noticeable effect on the radiance and irradiance spectra (Fig. 3), and consequently on the cross calibration spectra (Fig. 4) and NDVI. In particular, under cloudy conditions, the water absorption band near 970 nm was deeper for both the raw irradiance and radiance spectra (Fig. 3). Additionally, under diffuse, cloudy conditions (relative to sunny conditions), there were noticeable declines in the visible regions (particularly 500–700 nm) of the radiance spectra (Fig. 3B).

The cross-calibration spectra (ratio of calibration panel radiance to irradiance) were markedly different under the two conditions (Fig. 4B). However, when the appropriate cross-calibration spectra (Fig. 4B) were applied to the raw, uncorrected reflectance (Fig. 4A), the resulting corrected reflectance spectra (Fig. 4C) were remarkably similar to each other. In both cases, the slight bumps and dips present in the raw reflectance (Fig. 4A) were removed by the correction procedure. These slight features in the uncorrected reflectance spectra are artifacts primarily due to the different responses of the two detectors and their respective foreoptics, and the cross calibration procedure effectively removes these artifacts.

The slight differences in whole-ecosystem reflectance under clear and cloudy conditions (Fig. 4C) are presumably due to different degrees of radiation penetration into the vegetation stand under direct and diffuse light conditions. Under clouds, this light penetration is slightly greater, resulting in reduced reflectance across most of the spectrum (Fig. 4C). This results in a 12% higher NDVI (and consequently higher absorbed radiation) under cloudy relative to sunny conditions (Fig. 4C). This enhanced light penetration is one factor enhancing ecosystem photosynthetic light-use-efficiency under cloud cover, as has sometimes been noted in eddy covariance studies (e.g. Goulden et al., 1997). Because of their inability to penetrate thick clouds, optical satellite sensors are presumably unable to detect these effects of sky condition on NDVI.

In addition to sky conditions, we used the tram to explore the effects of time of day on whole-ecosystem reflectance and NDVI. These tests revealed striking diurnal NDVI patterns for this ecosystem, with the diurnal effect on NDVI greater than the seasonal effect (Fig. 5). Clearly, in this vegetation stand, as in many discontinuous vegetation stands where canopy gaps cause strong shadow effects, time of day exerts a strong influence on the apparent NDVI due to interactions between sun angle and stand structure. One way of correcting for this effect when

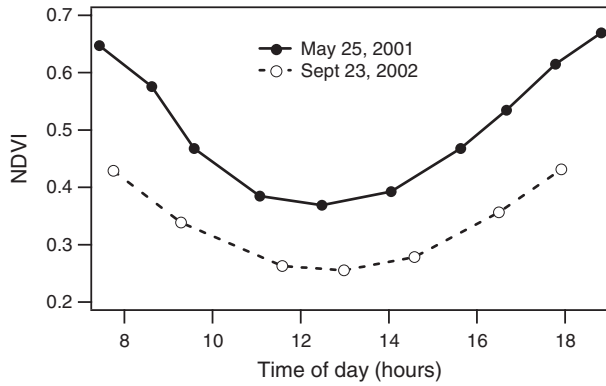


Fig. 5. Diurnal NDVI patterns for two dates: May 25, 2001 (during spring rains), and September 23, 2002 (during severe drought).

comparing NDVI values across dates is to express NDVI as a function of sun angle, then calculate a sun-angle-corrected NDVI value (see Sims et al., this issue, for a further discussion of this method). Clearly, when sampling seasonal patterns of NDVI, these confounding effects of sun angle and time of day need to be considered. In part to minimize the diurnal effect on NDVI, all further data presented here involve midday sampling only (values collected within an hour of solar noon).

Another useful feature of the tram is its ability to provide detailed spatial profiles of spectral reflectance and reflectance indices. The spatial patterns of NDVI along the 100-m tram line for several representative dates are shown in Fig. 6. These figures illustrate striking effects of species composition (associated with individual peaks along the tram), as well as disturbance (drought and fire) and recovery from disturbance. Under favorable conditions (May 25, 2001, before drought and fire), high NDVI values are associated with individual shrubs (*A. fasciculatum*, *A. sparsifolium*, and *A. pungens*), and troughs are associated with bare soil patches in between shrubs. Thus, the tram system sampling at 1 m grain sizes (“small pixels”) can resolve individual species patches in this mature chaparral stand. Representative reflectance spectra associated with the different shrub species along the transect are shown in Fig. 7.

The severe drought of 2002, the driest year on record for this site (unpublished data), caused severe declines in NDVI values for vegetated patches, but not for bare soil (Fig. 6A). This decline was associated with leaf drop, and the death of individual branches and shrubs. One species in particular, *A. pungens* (providing the biggest NDVI peak in Fig. 6A), did not survive the drought, leading to changes in species composition. This selective loss of this species due to drought was apparent by the lack of recovery in NDVI for this species (compare the tallest peak in Fig. 6A to the same position in Fig. 6B). By contrast, the other two dominant species (*A. fasciculatum* and *A. sparsifolium*) regrew their canopies after drought, leading to a general recovery in NDVI over most of the transect (Fig. 6B).

The next serious disturbance, a wildfire in July, 2003, killed virtually all above-ground vegetation, causing a dramatic “flattening” of the NDVI profile (Fig. 6B). With the return of winter rains, regrowth of the vegetation occurred so that by the spring of the next year (2004), NDVI had increased

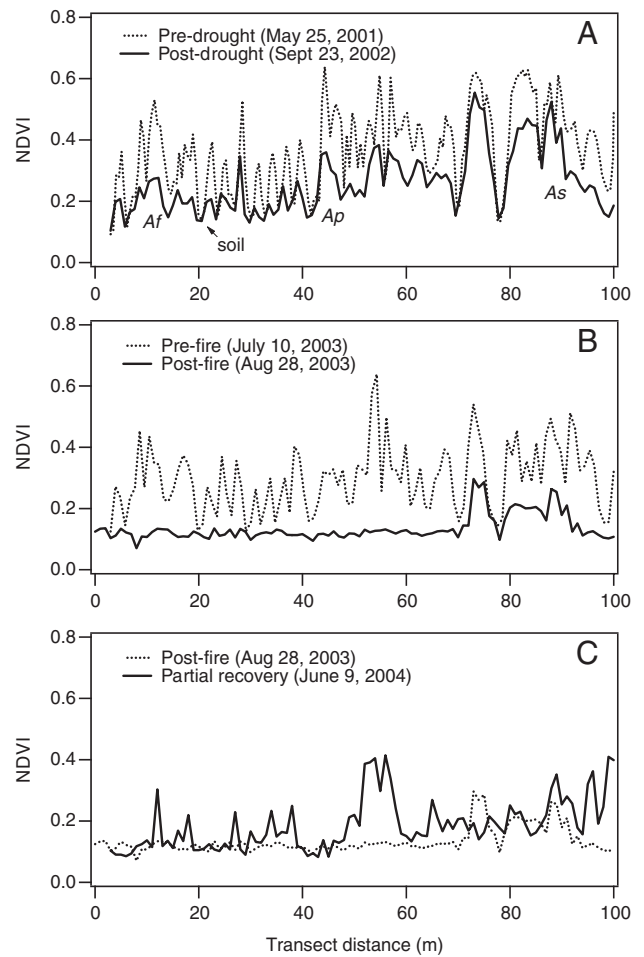


Fig. 6. Midday NDVI as a function of distance along the tram transect. Individual peaks represent individual chaparral shrubs (*A. fasciculatum* = Af, *A. sparsifolium* = As, *A. pungens* = Ap) The drought in 2002 resulted in considerable shrub dieback, visible as declines in individual peaks (transition from dotted to solid line, panel A). The fire in 2003 resulted in further loss of green biomass (solid line, panel B), followed by partial recovery due to postfire regrowth (solid line, panel C).

markedly from the post-fire state (Fig. 6C), with individual NDVI peaks associated with resprouting shrubs and patches of annual seedlings that germinated in the winter following fire.

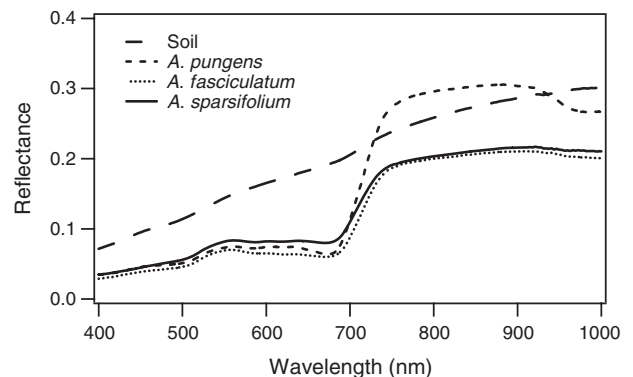


Fig. 7. Representative reflectance spectra for soil background (“soil”) and three dominant shrub species (*A. pungens*, *A. fasciculatum*, and *A. sparsifolium*). All spectra collected on May 25, 2001 at the transect positions indicated in Fig. 6A.

The post-fire resprouting is visible in Fig. 8, which shows a detail of Fig. 6C (meters 46–61) alongside photographs taken of the ground surface from the tram. The camera provides a photographic record that can be used for evaluating the contribution of individual cover types to the overall ecosystem reflectance signal.

Another way to express the tram data is to calculate an average reflectance for the ecosystem by averaging all the reflectance values along the tram line for a given date and then calculating a representative ecosystem NDVI value (“big-pixel” NDVI) for that date. The corresponding ecosystem-average reflectance spectra for the dates shown in Fig. 6 are plotted in Fig. 9, illustrating the dramatic effects of drought, fire and recovery on spectral reflectance, and thus on NDVI. In particular, drought caused a dramatic “flattening” of the reflectance spectra, particularly near the red edge (700 nm), due to the loss of green leaves (Fig. 9A). This flattening largely reversed due to vegetation regrowth with the onset of normal rainfall (see July 10, 2003 spectrum, Fig. 9B). The July 2003 wildfire removed almost all above-ground green vegetation and caused a second, more severe flattening of the reflectance spectrum (see August 28, 2003 spectrum, Fig. 9B), which again recovered due to regrowth following winter rains (see June 9, 2004 spectrum, Fig. 9B).

The impacts of season and disturbance (drought and fire) on average ecosystem NDVI are summarized in Fig. 10, which shows approximately 5 years of data collected along the tram transect. Several features are clearly visible in this time trend. First, a brief period of snow (winter 2001) caused a striking but transient dip in NDVI that disappeared upon snowmelt. This dip was not due to a change in actual vegetation greenness or leaf area index visible to the sensor; rather, it was due to the confounding effect of background snow cover on the whole-ecosystem NDVI signal.

The drought of 2002 (following record-low rainfalls in the winter of 2002) led to a clear decline in NDVI by midsummer. The apparent recovery in NDVI towards the end of 2002 is largely due to sun-angle effects, which cause an increase in apparent NDVI at low sun angles (e.g. early and late times of the day, and the winter solstice, see Fig. 5 and Sims et al., this issue, for a discussion of this effect). Actual canopy regrowth

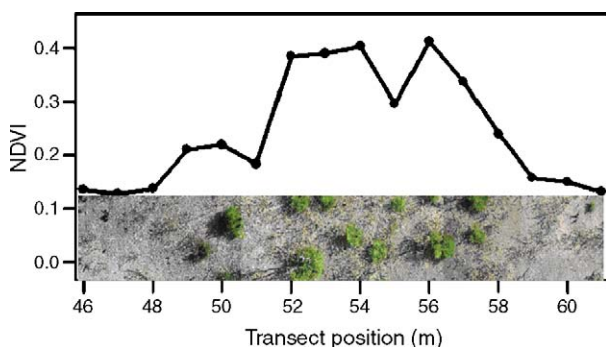


Fig. 8. Detail from Fig. 6 (June 9, 2004), showing region of peak NDVI due to shrub resprouting, visible in the photos on the bottom of the figure. Also visible are recently senesced annuals (grey–brown vegetation).

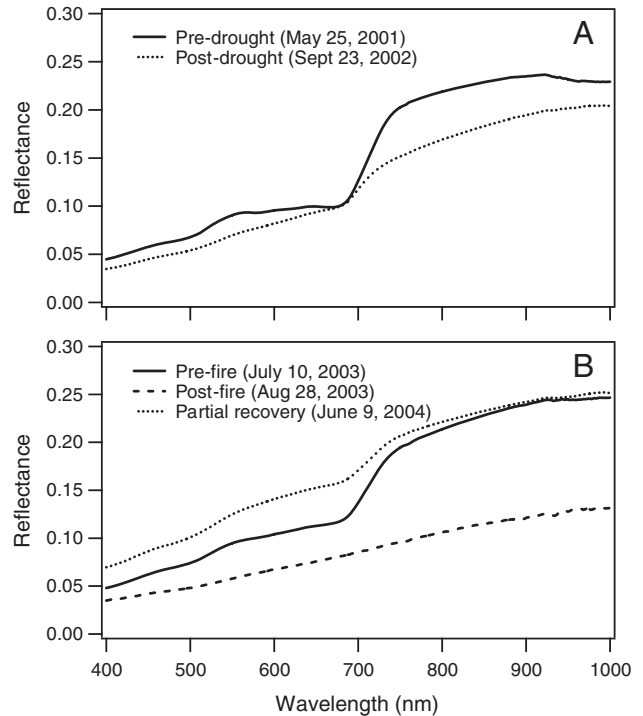


Fig. 9. Average ecosystem reflectance for the different dates (before and after drought and fire) shown in Fig. 6. In this case, reflectance represents the average reflectance for the entire tram transect (100 positions).

following the return of normal rainfall in winter, 2003, led to a peak in NDVI by June, 2003 (Fig. 10).

This maximum NDVI value was quickly and dramatically reduced by the July 2003 wildfire. The gradual upward trend in NDVI following the fire indicates vegetation regrowth, with peak NDVI values associated with the timing of maximum greenness of spring annuals in 2004 and 2005 (Fig. 10). The ephemeral nature of these springtime, post-fire NDVI peaks were a result of the rapid growth and desiccation of this post-fire annual vegetation, which is a common chaparral feature.

Also visible in the figure are slight “bumps” or “dips” in an otherwise smooth NDVI trend. These features are partly attributable to changing sky conditions (clear vs. overcast), which

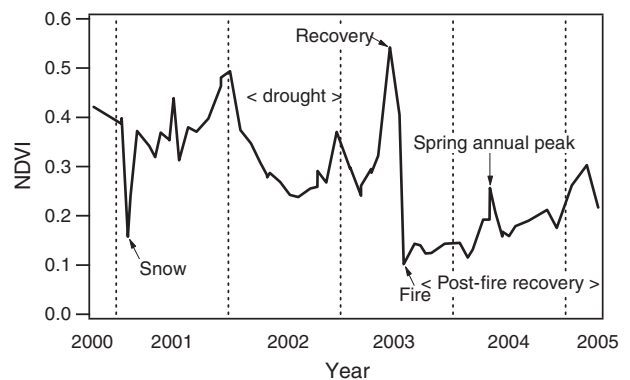


Fig. 10. Five years of NDVI at Sky Oaks, CA measured by the tram. In this case, NDVI represents the ecosystem-average NDVI measured at midday with a nadir view. Periods of snow, drought, post-drought recovery, fire, post-fire recovery and spring annual activity are indicated.

can cause slight deviations in apparent NDVI (see explanation of Fig. 4, above).

4. Discussion and conclusion

The robotic tram provides an effective, systematic way of sampling ecosystem spectral reflectance with great precision, allowing the same landscape positions to be sampled through time. Although nominally “evergreen,” this ecosystem’s optical properties and resultant NDVI proved to be remarkably dynamic over space and time. Many abiotic factors, including temporary snow cover, sky conditions (cloudy vs. clear), time of day (due to sun angle and canopy/stand structure), and season (partly due to sun angle) had marked influence on this index. Additional factors affecting NDVI were the result of rain, drought, fire, secondary succession (shrub regrowth and annual vegetation growth) and associated changes in species composition and stand structure. The systematic sampling of the tram system allow these effects to be experimentally separated, and provided a powerful means for understanding the factors controlling surface-atmosphere carbon and water vapor fluxes. The actual links between these perturbations and carbon and water vapor fluxes for this site are explored in separate studies (Claudio et al., *this issue*; Fuentes et al., 2006-*this issue*; Sims et al., 2006-*this issue*).

The challenge of interpreting NDVI (or any reflectance index) lies in understanding and separating the many factors that influence it. NDVI is generally considered a “greenness” index for estimation of vegetation absorbed radiation (APAR, Gamon & Qiu, 1999; Sims et al., *this issue*), and ideally it would only detect properties related to green leaf area index and APAR. However, as shown here, multiple factors not related to greenness per se (e.g. background snow cover, time of day, and atmospheric light conditions) affect the retrieved NDVI and thus our interpretation of ecosystem biological activity and light absorption.

There are several potential solutions to this multi-factor problem. One might be to develop alternative indices that reduce some of these confounding effects. An example is the Enhanced Vegetation Index (EVI, Huete et al., 2002), that is showing promise as an index of carbon flux for different ecosystems (Rahman et al., 2005), and that also tracks vegetation changes in this ecosystem (Cheng et al., *this issue*). Another is to use the full spectral information to identify the multiple factors involved, to model spectral reflectance accordingly, and remove confounding factors (e.g. structural or background effects), leaving a “purer” vegetation greenness signal (Asner & Heidebrecht, 2005). However, this method requires a full-range (short-wave infrared) spectrometer, which was not available here. Preliminary field tests (not shown) have indicated the potential for running full-range spectrometers from this mobile platform, but normally the high cost, large mass, and extensive maintenance requirements of these spectrometers preclude their routine use for this application. Thus, a full exploration of these alternatives was beyond the scope of this study.

This chaparral site is normally considered “evergreen” because many of the dominant species retain most of their leaves through the year in a normal year (Stylinski et al., 2002). However, the sampling period of this study included two unusual

events, including a record drought (2002) and wildfire (2003), both of which had marked impacts on leaf-area index, green vegetation cover, species composition, and thus NDVI. The ecosystem proved to be remarkably resilient, with many species regrowing following drought and fire, however, these events also caused marked changes in leaf area index, vegetation cover, and species composition that were detectable with the tram system. These observations reveal a common aspect of arid and semi-arid sites in general, and that is their remarkable dynamism, which is reflected in the particularly dynamic flux responses for this site (Claudio et al., 2006-*this issue*; Fuentes et al., 2006-*this issue*). The profound changes in biological activity in response to perturbations, and thus in optical properties and fluxes, make arid and semi-arid sites particularly useful for revealing controls on surface-atmosphere fluxes.

A useful application of the tram’s multi-temporal sampling ability is in evaluating satellite products. Satellite validation has been explored in a separate study (Cheng et al., *this issue*). Other applications (not explored here) include multi-angle sampling for exploration of ecosystem bidirectional reflectance distribution function (BRDF), which is proving a useful indicator of stand structure and vegetation type (Gamon et al., 2004).

Due to the requirement for supporting track, the above-canopy sampling ability of the tram is limited to short-statured vegetation. In our experience, it becomes difficult to support and maintain a track at heights much greater than about 4–5 m, so this appears to represent an upper height limit for this sampling method. For taller vegetation, other mobile platforms (e.g. cable-mounted systems, blimps, aircraft, or UAVs) may be more appropriate. The tram has now also been successfully applied in an arctic tundra ecosystem (Stow et al., 2004), and a current goal is to establish tram systems at a number of SpecNet sites having short-statured vegetation. A concluding recommendation is the establishment of similar continuous optical monitoring systems across a wider range of flux tower sites and ecosystems. This would provide a valuable network for exploring ecosystem optical properties related to surface-atmosphere fluxes. The SpecNet network is beginning to provide this.

Acknowledgements

Development of the tram was made possible by NSF (CREST, SGER and Ecosystems) and IARC grants to J.A.G. Thanks to the staff of the Sky Oaks Field Station and the San Diego State University Field Stations Office for their support of this project. Administrative support for tram development was provided by the Desert Research Institute, Reno NV, USA. J. Cano, F. Chowdhury, D. Horyath, and R. Johnson provided technical assistance. Z. Mao and D. Thayer provided assistance with Fig. 8.

References

- Asner, G. P., & Heidebrecht, K. B. (2005). Desertification alters regional ecosystem-climate interactions. *Global Change Biology*, *11*, 182–194.
- Baldocchi, D., Falge, E., Gu, L., Olson, R., Hollinger, D., Running, S., et al. (2001). FLUXNET: A new tool to study the temporal and spatial variability

- of ecosystem-scale carbon dioxide, water vapor, and energy flux densities. *Bulletin of the American Meteorological Society*, 82(11), 2415–2434.
- Baldocchi, D. D., Hincks, B. B., & Meyers, T. P. (1988). Measuring biosphere–atmosphere exchanges of biologically-related gases with micrometeorological methods. *Ecology*, 69, 1331–1340.
- Baldocchi, D. D., Law, B. E., & Anthoni, P. M. (2000). On measuring and modeling energy fluxes above the floor of a homogenous and heterogenous conifer forest. *Agricultural and Forest Meteorology*, 102, 187–206.
- Claudio, H. C., Cheng, Y., Fuentes, D. A., Gamon, J. A., Luo, H., Oechel, W., et al. (2006). Monitoring drought effects on vegetation water content and fluxes in chaparral with the 970 nm water band index. *Remote Sensing of Environment*, 103, 304–311 (this issue). doi:10.1016/j.rse.2005.07.015
- Cheng, Y., Gamon, J. A., Fuentes, D. A., Mao, Z., Sims, D. A., Qui, H. -L., et al. (2006). A multi-scale analysis of dynamic optical signals in a Southern California chaparral ecosystem: A comparison of field, AVIRIS and MODIS data. *Remote Sensing of Environment*, 103, 369–378 (this issue). doi:10.1016/j.rse.2005.06.013
- Fuentes, D. A., Gamon, J. A., Cheng, Y., Qui, H. -L., Mao, Z., Sims, D. A., et al. (2006). Mapping carbon and water vapor fluxes in a chaparral ecosystem using vegetation indices derived from AVIRIS. *Remote Sensing of Environment*, 103, 312–323 (this issue). doi:10.1016/j.rse.2005.10.028
- Gamon, J. A., Huemmrich, K. F., Peddle, D. R., Chen, J., Fuentes, D., Hall, F. G., et al. (2004). Remote sensing in BOREAS: Lessons learned. *Remote Sensing of Environment*, 89, 139–162.
- Gamon, J. A., & Qiu, H. -L. (1999). Ecological applications of remote sensing at multiple scales. In F. I. Pugnaire & F. Valladares F. (Eds.), *Handbook of functional plant ecology* (pp. 805–846). New York: Marcel Dekker, Inc.
- Gamon, J. A., Rahman, A. F., Dungan, J., Schildhauer, M., & Huemmrich, K. F. (2006). Spectral Network (SpecNet)—What is it and why do we need it? *Remote Sensing of Environment*, 103, 227–235 (this issue). doi:10.1016/j.rse.2006.04.003
- Goulden, M. L., Daube, B. C., Fan, S. M., Sutton, D. J., Bazzaz, A., Munger, J. W., et al. (1997). Physiological responses of a black spruce forest to weather. *Journal of Geophysical Research*, 102(D24), 28987–28996.
- Huete, A., Didan, K., Miura, T., Rodriguez, E. P., Gao, X., & Ferreira, L. G. (2002). Overview of the radiometric and biophysical performance of the MODIS vegetation indices. *Remote Sensing of Environment*, 83, 195–213.
- Malmstrom, C. M., Thompson, M. V., Juday, G. P., Los, S. O., Randerson, J. T., & Field, C. B. (1997). Interannual variation in global-scale net primary production: Testing model estimates. *Global Biogeochemical Cycles*, 11(3), 367–392.
- Moncreiff, J. B., Malhi, Y., & Leuning, R. (1996). The propagation of errors in long-term measurements of land-atmosphere fluxes of carbon and water. *Global Change Biology*, 2, 231–240.
- Rahman, A. F., Gamon, J. A., Sims, D. A., & Schmidts, M. (2003). Optimal pixel size for hyperspectral remote sensing of ecosystem function: A case study of Southern California grassland and chaparral. *Remote Sensing of Environment*, 84, 192–207.
- Rahman, A. F., Sims, D. A., Cordova, V. D., & El-Masri, B. Z. (2005). Potential of MODIS EVI and surface temperature for directly estimating per-pixel ecosystem C fluxes. *Geophysical Research Letters*, 32, L19404, doi:10.1029/2005GL024127
- Running, S. W., Baldocchi, D. D., Turner, D. P., Gower, S. T., Bakwin, P. S., & Hibbard, K. A. (1999). A global terrestrial monitoring network integrating tower fluxes, flask sampling, ecosystem modeling, and EOS satellite data. *Remote Sensing of Environment*, 70, 108–127.
- Running, S. W., Nemani, R. R., Heinsch, F. A., Zhao, M., Reeves, M., & Hashimoto, H. (2004). A continuous satellite-derived measure of global terrestrial primary production. *BioScience*, 54, 547–560.
- Sellers, P. J., Los, S. O., Tucker, C. J., Justice, C. O., Dazlich, D. A., Collatz, G. J., et al. (1996). A revised land surface parameterization (SiB2) for atmospheric GCMs, II. The generation of global fields of terrestrial biophysical parameters from satellite data. *Journal of Climatology*, 9(4), 706–737.
- Sims, D. A., Luo, H., Hastings, S., Oechel, W. C., Rahman, A. F., & Gamon, J. A. (2006). Parallel adjustments in vegetation greenness and ecosystem CO₂ exchange in response to drought in a Southern California chaparral ecosystem. *Remote Sensing of Environment*, 103, 289–303 (this issue). doi:10.1016/j.rse.2005.01.020
- Stow, D. A., Hope, A., McGuire, D., Verbyla, D., Gamon, J., Huemmrich, F., et al. (2004). Remote sensing of vegetation and land-cover change in arctic tundra ecosystems. *Remote Sensing of Environment*, 89, 281–308.
- Stylinski, C. D., Gamon, J. A., & Oechel, W. C. (2002). Seasonal patterns of reflectance indices, carotenoid pigments and photosynthesis of evergreen chaparral species. *Oecologia*, 131, 366–374.
- Tans, P. P., Fung, I. Y., & Takahashi, T. (1990). Observational constraints on the global atmospheric CO₂ budget. *Science*, 247, 1431–1438.